LETTERS
PUBLISHED ONLINE: 8 NOVEMBER 2009 | DOI: 10.1038/NMAT2568
nature materials

Quasi-ballistic thermal transport from nanoscale interfaces observed using ultrafast coherent soft X-ray beams

Mark E. Siemens[1]*, Qing Li[1], Ronggui Yang[2], Keith A. Nelson[3], Erik H. Anderson[4], Margaret M. Murnane[1] and Henry C. Kapteyn[1]

Fourier theory of thermal transport considers heat transport as a diffusive process where energy flow is driven by a temperature gradient. However, this is not valid at length scales smaller than the mean free path for the energy carriers in a material, which can be hundreds of nanometres in crystalline materials at room temperature. In this case, heat flow will become 'ballistic'—driven by direct point-to-point transport of energy quanta[1]. Past experiments have demonstrated size-dependent ballistic thermal transport through nanostructures such as thin films, superlattices, nanowires and carbon nanotubes[1–8]. The Fourier law should also break down in the case of heat dissipation from a nanoscale heat source into the bulk. However, despite considerable theoretical discussion and direct application to thermal management in nanoelectronics[2], nano-enabled energy systems[9,10] and nanomedicine[11], this non-Fourier heat dissipation has not been experimentally observed so far. Here, we report the first observation and quantitative measurements of this transition from diffusive to ballistic thermal transport from a nanoscale hotspot, finding a significant (as much as three times) decrease in energy transport away from the nanoscale heat source compared with Fourier-law predictions.

When heat flows from a hotspot with a dimension L smaller than the mean free path of phonons in the heat sink Λ, energy-carrying phonons travel ballistically away from the source for a significant distance before experiencing collisions. However, in a Fourier picture of thermal transport, heat flow is assumed to be diffusive (experiencing many collisions), with the thermal flux q determined by the temperature gradient ($q \sim \nabla T$). When there is a significant energy density change over a distance less than Λ, there is no local phonon equilibrium and therefore temperature cannot be defined, as illustrated in Fig. 1a. Under these circumstances, the Fourier law, which assumes local thermal equilibrium, overestimates the thermal transport[1,12,13].

In the intermediate case when the hotspot dimension L is of the order of Λ, transport is neither fully ballistic nor diffusive. The full Boltzmann transport equation for phonons must then be solved to model thermal transport[1]. Unfortunately, an analytical solution of the Boltzmann transport equation for real systems is usually impractical without some simplifying assumptions, and numerical simulations vary widely in their prediction of the strength of this nanoscale hotspot effect[14–16]. Several phenomenological models have been proposed to explain the reduction in thermal flux for a nanoscale heat source, but there is significant variation in their predictions[17–19]. One model, the ballistic–diffusive equation model[17], provides clear insight by separating the size-dependent heat flux into contributions from ballistic and diffusive components, similar to what is done in the case of rarefied gas[20] or electron flow[21]. Figure 2 illustrates the predictions of this model qualitatively: at large length scales, the thermal transport is dominated by the Fourier component, but as the dimension of the hotspot is reduced, ballistic transport becomes increasingly important. Other models suggest that the transport is determined by different effects, such as non-propagating phonon modes[22] and interface effects[19]. This extensive modelling effort has, however, taken place in an absence of real experimental data with which to benchmark the models. Given the variations between these models, quantitative experiments are very important, both for a fundamental understanding of the basic and important phenomenon of heat flow, and to benchmark models of nanoscale heat transfer for nanosystem design.

In many practical nanosystems, an interface separates a small heated region from a heat-sink substrate, and the thermal resistance of this interface must also be taken into account. The heat flow from the heated nanostructure, as shown in Fig. 1a, can then be characterized by an effective resistance acting at the interface—with contributions from both a ballistic correction to the Fourier law and the conventional thermal boundary resistance (TBR) characterizing interfacial transport at bulk length scales. TBR is measured in thin films using time-resolved optical pump–probe methods such as transient thermoreflectance[4,23] (TTR). However, the diffraction limit for the visible probe light limits this technique to structures with linewidths greater than ~1 μm—too large in scale to observe ballistic size effects from a nanoscale heat source at room temperature. Using a specialized geometry that allowed confined heating without a heterogeneous material interface, Sverdrup *et al.* used electrical resistance thermometry to measure steady-state temperature distributions in a thin 5 μm silicon membrane near a 300-nm-wide highly doped silicon resistor. At temperatures below 200 K, they observed a slight deviation from the prediction of Fourier heat conduction[22]. However, this experiment did not allow for any systematic and quantitative comparison between experiment and theory owing to the limitations posed by the sample geometry. More recent work did not observe any ballistic size effect at room temperature[24]. It is worth noting however, that all of these measurements were

[1]JILA, University of Colorado at Boulder, Boulder, Colorado 80309, USA, [2]Department of Mechanical Engineering, University of Colorado, Boulder, Colorado 80309, USA, [3]Department of Chemistry, MIT, Cambridge, Massachusetts 02139, USA, [4]Lawrence Berkeley Labs and Center for X-ray Optics, Berkeley, California 94720, USA. *e-mail: siemens@colorado.edu.

Report Documentation Page

Form Approved
OMB No. 0704-0188

1. REPORT DATE	2. REPORT TYPE	3. DATES COVERED
JAN 2010		**00-00-2010 to 00-00-2010**

4. TITLE AND SUBTITLE	5a. CONTRACT NUMBER
Quasi-ballistic thermal transport from nanoscale interfaces observed using ultrafast coherent soft X-ray beams	5b. GRANT NUMBER
	5c. PROGRAM ELEMENT NUMBER
6. AUTHOR(S)	5d. PROJECT NUMBER
	5e. TASK NUMBER
	5f. WORK UNIT NUMBER
7. PERFORMING ORGANIZATION NAME(S) AND ADDRESS(ES) **University of Colorado,JILA and Department of Physics,Boulder,CO,80309**	8. PERFORMING ORGANIZATION REPORT NUMBER
9. SPONSORING/MONITORING AGENCY NAME(S) AND ADDRESS(ES)	10. SPONSOR/MONITOR'S ACRONYM(S)
	11. SPONSOR/MONITOR'S REPORT NUMBER(S)

12. DISTRIBUTION/AVAILABILITY STATEMENT
Approved for public release; distribution unlimited

13. SUPPLEMENTARY NOTES

14. ABSTRACT

15. SUBJECT TERMS

16. SECURITY CLASSIFICATION OF:			17. LIMITATION OF ABSTRACT	18. NUMBER OF PAGES	19a. NAME OF RESPONSIBLE PERSON
a. REPORT **unclassified**	b. ABSTRACT **unclassified**	c. THIS PAGE **unclassified**	**Same as Report (SAR)**	**5**	

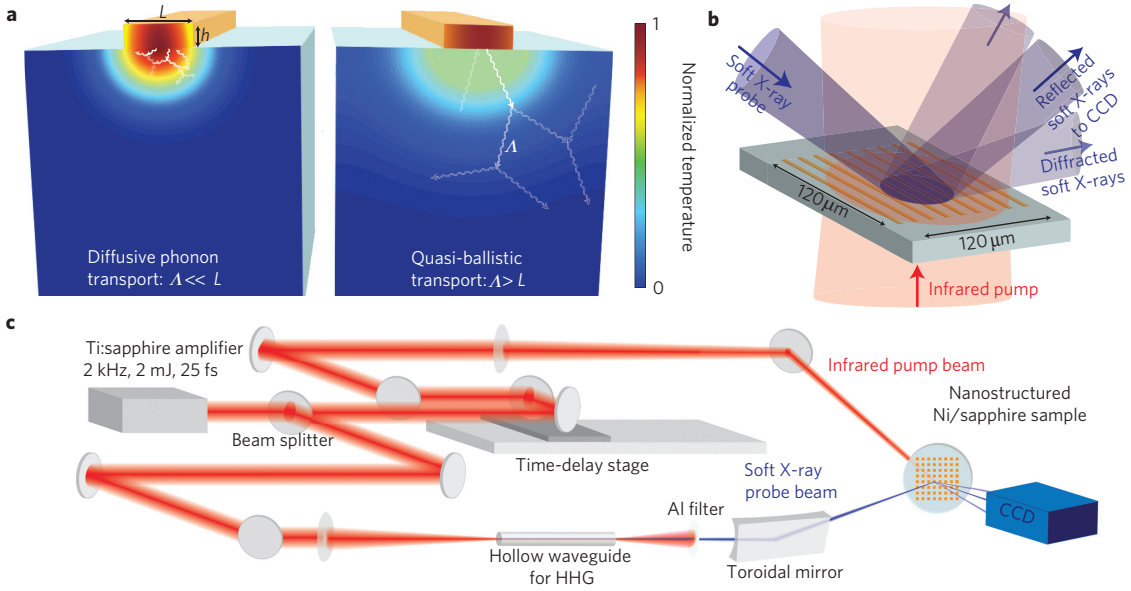

Figure 1 | Experimental set-up for measuring thermal transport across a nanoscale interface. a, Schematic illustrating the difference between diffusive and quasi-ballistic thermal transport across an interface. When the size of the interface is less than the phonon mean path in the substrate, the Fourier diffusive heat equation breaks down. **b**, Sample geometry showing infrared laser illumination and soft X-ray detection scheme. **c**, Experimental geometry: an infrared laser beam at 800 nm heats the nanostructure, and a soft X-ray beam at 29 nm monitors the heat flow from the nanostructure into the substrate.

done using steady-state techniques poorly suited to capturing short-timescale ballistic dynamics.

In this work, we use a beam of ultrafast coherent soft X-rays, at a wavelength of 29 nm, to directly observe the cooling dynamics of a nanoscale heat source into its bulk surroundings. By interferometrically monitoring displacement in a heated nanostructure using diffraction of soft X-ray light, we can detect dynamic temperature changes more sensitively than would be possible using either ultrashort optical pulse probing or steady-state measurements. This ultrafast short-wavelength transient-diffraction methodology represents a newly developed experimental capability that allows us to map out nanoscale thermal transport over a range of nanostructure sizes.

Figure 1a illustrates the difference between diffusive and ballistic heat transfer, and Fig. 1b,c shows the sample geometry and overall experimental set-up. Periodic nickel lines with a height of 20 nm, length of 120 μm and with widths L varying from 65 to 2,000 nm were fabricated on a sapphire substrate using electron beam lithography and a lift-off process (at a fixed linewidth-to-period ratio of 25%). An identical nickel nanostructure was prepared on a fused-silica reference substrate. As discussed in Supplementary Section S1, compared with fused silica (which has an averaged mean free path for heat-carrying phonons of ~2 nm), the averaged mean free path of heat-carrying phonons in sapphire is of the order of 100–150 nm at room temperature. All experiments were carried out at room temperature and in high vacuum (~10^{-6} torr). The nickel lines were impulsively heated by ultrashort (25 fs) pulses from a high-power Ti:sapphire laser-amplifier system. Pump pulses at a wavelength of 800 nm were focused to a fluence of 2.5 mJ cm^{-2}, in a spot roughly five times the size of the nanostructured nickel sample to ensure uniform heating. Owing to the high transmission of the sapphire and fused-silica substrates at 800 nm, only the nanostructure was heated.

To probe the heat flow dynamics, an ultrafast, coherent soft X-ray beam is diffracted from the nanostructure at a variable pump–probe time delay. The soft X-ray beam is generated through the high-order harmonic generation (HHG) process[25] by focusing ~1 mJ pulses from the Ti:sapphire amplifier into a hollow

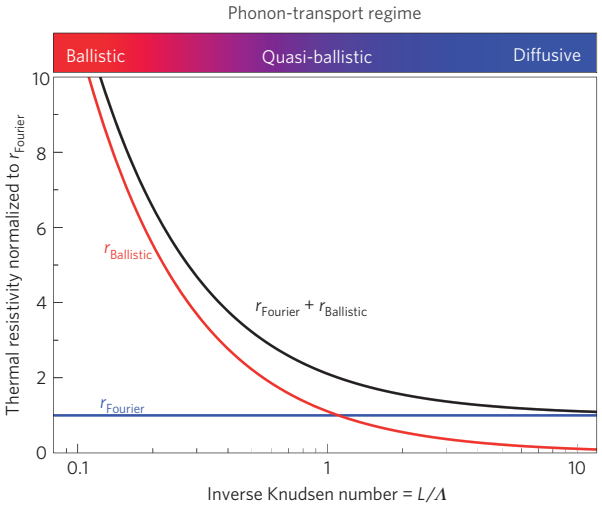

Figure 2 | Analytical prediction of the Fourier and ballistic components of the resistivity for thermal transport away from a half-cylinder of diameter *L*. When the linewidth L is much larger than the phonon mean free path Λ, the Fourier component (blue) is the largest, but for $L < \Lambda$, the ballistic resistivity (red) is dominant. Figure 4 shows the first measurement of the ballistic correction to the Fourier resistivity.

waveguide filled with argon gas. The resulting nonlinear interaction between the intense laser pulses and the atoms in the gas generates odd harmonics of the driving laser frequency. Absorption of the argon gas and aluminium filters (used to block the residual 800 nm light) eliminate all but the 25th, 27th and 29th harmonic orders, with a spectrum peaked at 29 nm. The full spatial coherence and short wavelength of the soft X-ray beams from the waveguide make them ideal for highly sensitive interferometric measurements of nanoscale surface deformation[26]. Furthermore, the very short duration of the HHG pulses (sub-10 fs; ref. 27) makes possible unprecedented temporal resolution for dynamics experiments. The soft X-ray harmonics are refocused to a ~100 μm spot on the sample

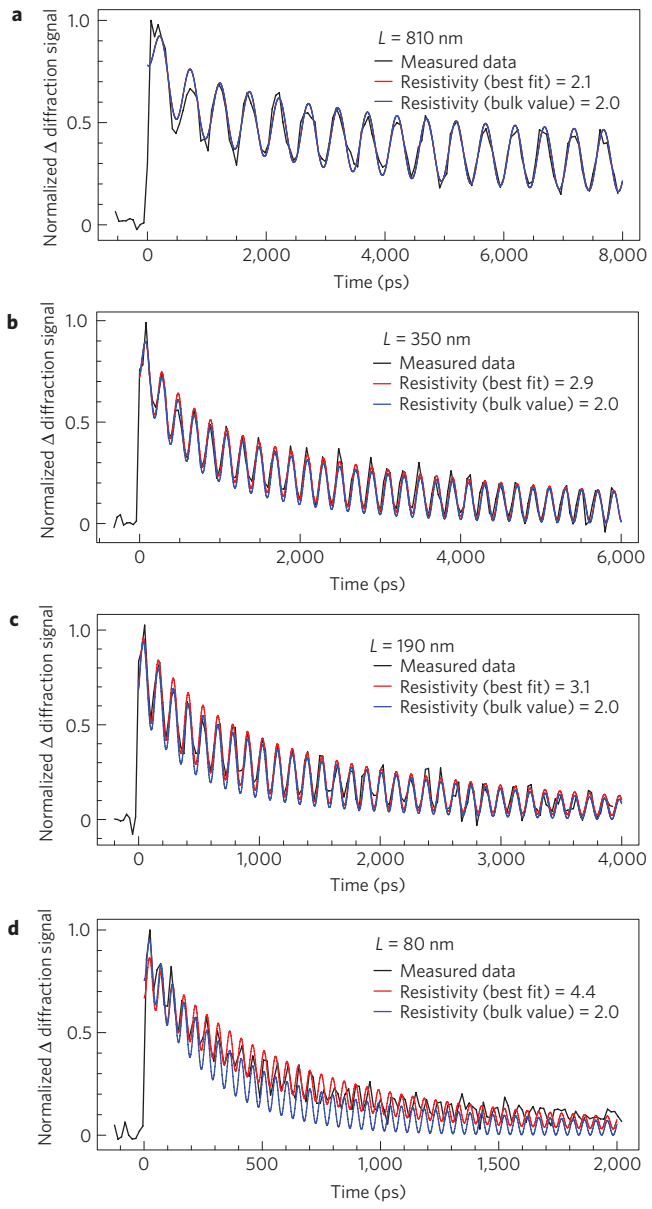

Figure 3 | Normalized dynamic soft X-ray diffraction signal for Ni lines on sapphire. a–d, Ni linewidths are 810 nm (**a**), 350 nm (**b**), 190 nm (**c**) and 80 nm (**d**). The signal in each case consists of a sharp rise owing to impulsive laser heating, a thermal decay owing to interfacial thermal transport and an oscillation owing to surface acoustic wave propagation. The red and blue curves show the fit using the Fourier law for thermal transport in the substrate and either large-scale interfacial resistance (blue) or a modified effective interfacial resistance ($r_{Effective}$, units of 10^{-9} K m^2 W^{-1}), which accounts for ballistic effects from a nanoscale heat source (red). The deviation between the two fits increases with decreasing linewidth.

using a grazing-incidence toroidal mirror. The HHG beam reflected and diffracted from the nanostructure is then recorded using a CCD (charge-coupled device) camera (Fig. 1b).

The change in soft X-ray probe diffraction as a function of delay after the infrared heating pulse for varying nickel linewidth is shown in Fig. 3. The signal decays as the heat in the nickel nano-lines dissipates into the substrate. The rate of this thermal decay depends on the thermal transport across the nickel/substrate interface and in the substrate. The rapid oscillations in the signal are due to surface acoustic wave (SAW) propagation in the nanostructure. Periodic surface strain caused by the patterned heating generates the SAW; we confirm that this is the source of the oscillations by comparing the measured frequency of oscillation with the Rayleigh velocity for SAW propagation in the substrate[28].

To interpret our results, we use an analysis similar to that used for TTR measurements of interfacial thermal resistivity. To extract the cooling dynamics of the nickel nanostructure from data shown in Fig. 3, we implemented a multiphysics model including thermal transport, thermomechanics and Fresnel optical propagation (see Supplementary Section S2). The model takes the full two-dimensional geometry into account. First, thermal transport across the interface is governed by the conservation of energy across the surface, where x and y are along and away from the surface respectively

$$\rho_{Ni} h_{Ni} C_{Ni} \frac{dT_{Ni}(x,t)}{dt} = -\frac{(T_{Ni}(x,t) - T_s(x,y=0,t))}{r_{Effective}}$$

where $r_{Effective}$ is the interface resistivity that will be modified later to include ballistic effects away from the interface, ρ_{Ni} and C_{Ni} are the density and volumetric specific heat in the nanostructure, respectively and, T_{Ni} and T_s are the time- and position-dependent temperatures in the nanostructure and substrate, respectively. Heat propagation is modelled by numerically solving the heat equation

$$\frac{\partial T_s(x,y,t)}{\partial t} = \frac{k_s}{C_s} \nabla^2 T_s(x,y,t) \quad (1)$$

in the substrate beneath a single nickel line using periodic boundary conditions to account for the neighbouring lines. In equation (1), k_s and C_s are the thermal conductivity and volumetric specific heat of the substrate respectively. Second, thermal expansion of the substrate surface Δh_s is calculated from the thermoelastic equation assuming a stress-free interface[29], which involves a weighted summation over the temperature distribution at each point

$$\Delta h_s(x) = 2\frac{(1+\nu_s)\alpha_s}{3\pi} \int_{x_1}\int_{y} T(x_1,y) \frac{y\,dx\,dy}{(x-x_1)^2+y^2}$$

where α_s is the coefficient of linear thermal expansion of the substrate and ν_s is Poisson's ratio. Thermal expansion of the nickel lines is also accounted for using $\Delta h_{Ni}(x) = \alpha_{Ni} T_{Ni}(x)$. Finally, Fresnel optical propagation and diffraction from the resulting surface profile gives the relative signal contributions from the nickel lines and the substrate. We parameterize the results of this numerical model in terms of an effective resistivity $r_{Effective}$ that acts at the interface and includes both conventional thermal boundary resistivity and size-dependent ballistic effects in the substrate owing to the confined heat source, and fit to the time-resolved thermal decay data. We use the parameter resistivity (r, units m^2 K W^{-1}) rather than the resistance (R, units K W^{-1}), as the latter depends on the contact area of the nanostructured interface.

To qualitatively understand the nature of the ballistic thermal transport, we modified the model proposed by Chen for heat flow from a nanoscale sphere into an infinite substrate[13], which separately calculates the diffusive and ballistic contributions to the total flux[17]. We implemented the model using a cylindrical geometry and extracted the resistivity, which is inversely proportional to the heat flux. Details of our model are given in Supplementary Section S3. The results, shown in Fig. 2, illustrate the nature of the quasi-ballistic heat-transfer effect as a function of the inverse Knudsen number L/Λ. For linewidths larger than the mean free path, the resistivity predicted by the Fourier law dominates and the

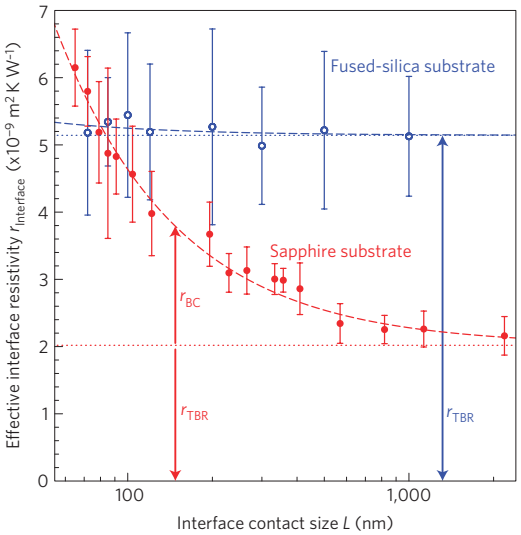

Figure 4 | Measured effective thermal resistivity for nickel nanostructures of width *L* deposited on fused-silica and sapphire substrates. The blue and red dotted horizontal lines show the large-scale resistivity r_{TBR} for data from the fused-silica and sapphire substrates. The blue and red dashed curves show model predictions for the ballistic resistivity correction $r_{BC} \sim \Lambda/L$, with $\Lambda_{FS} = 2$ nm and $\Lambda_{Sa} = 120$ nm, respectively. The error bars indicate the standard deviation in the fits to the data.

ballistic resistivity is negligible. However, when the dimension of the heated interface is comparable to or smaller than the phonon mean free path in the substrate, the Fourier law significantly under-predicts the resistivity (or over-predicts the heat flux). The under-prediction in the Fourier law is given by $r_{Ballistic}/r_{Fourier}$, so we introduce a ballistic correction resistivity r_{BC} proportional to this ratio (and therefore proportional to Λ/L), as shown by the red line in Fig. 2. The Fourier resistivity, $r_{Fourier}$, is automatically accounted for in our numerical model for heat propagation in the substrate (equation (1)). We combine the ballistic correction with the size-independent thermal boundary resistivity for transport across the interface to get an effective resistivity given by

$$r_{Effective} = r_{TBR} + r_{BC}$$

In our analyses, we extract the effective resistivity $r_{Effective}$ for each linewidth from the best fits (minimized root mean squared error) to our data. By definition, large linewidth measurements on both samples yield the large-scale values of thermal boundary resistivity r_{TBR} (equivalent to TTR measurements of thermal boundary resistance on thin films), as shown by the horizontal dotted lines in Fig. 4. The ballistic correction r_{BC} is given by the deviation of the measured resistivity at a given linewidth from the resistivity r_{TBR} measured at large linewidths L. The best fits to the data shown in Fig. 3 (red lines) demonstrate that the measured interface resistivity increases as the heated region gets smaller. The measured values of $r_{Effective}$, r_{TBR} and r_{BC} for both sapphire and fused-silica substrates are shown in Fig. 4. We measure a small deviation from r_{TBR} for the fused-silica substrate, because the averaged phonon mean free path in fused silica $\Lambda_{FS} \sim 2$ nm is much shorter than the smallest nickel linewidths. However, in the case of heat transfer from nanostructures deposited on sapphire substrates, the extracted resistivity at the smallest linewidths is more than three times higher than the large-scale value. The blue dotted and red dashed lines in Fig. 4 show the predicted resistivity values $r_{Effective}$ (with $r_{BC} = r_{Effective} - r_{TBR}$ proportional to Λ/L) based on the analytical ballistic–diffusive model (Fig. 2). The best fits to the experimental data give estimates of the average phonon mean free paths of $\Lambda_{FS} = 2$ nm (upper limit of ~5 nm beyond which a good fit is no longer possible) and $\Lambda_{Sa} = 120 \pm 10$ nm. As discussed above and in Supplementary Section S4, these values compare well to the expected value of Λ.

Our measurements demonstrate that the physical fundamentals of phonon transport from a nanoscale heat source can be understood by considering a minimum heated region model[13], which proposes that Fourier transport can be corrected by requiring the length scale of the heat source to be larger than the phonon mean free path: $L \rightarrow L + \Lambda$. The effective resistivity correction in this case is $(1 + \Lambda/L)$, which is the experimental dependence we observed, shown as the red dashed line in Fig. 4. This implies that heat flow from a nanoscale heat source smaller than the phonon mean free path can be thought of as emerging from a larger spot corresponding to the size of the phonon mean free path in the substrate.

This is the first direct and systematic measurement of quasi-ballistic thermal transport effects from a nanoscale heated region. We observe the breakdown of conventional Fourier heat conduction from interfaces smaller than the phonon mean free path Λ. We find excellent agreement between the experimental data and an analytical model that determines the thermal transport by summing the ballistic and diffusive contributions, and demonstrate that the Fourier law can still be used if corrected with an extra size-dependent resistance, proportional to the Knudsen number Λ/L, accounting for ballistic effects. Ballistic effects are expected to get even stronger as nanostructures shrink in size or for silicon substrates with even longer mean free paths ($\Lambda_{Si} \sim 250$ nm). These experiments thus advance the understanding of heat-transfer fundamentals, and are important for the design and manipulation of nanoscale thermal transport in circuits, thermoelectrics, photovoltaics and other structures of interest in nanotechnology.

Received 22 July 2009; accepted 6 October 2009; published online 8 November 2009

References

1. Chen, G., Borca-Tasciuc, D. & Yang, R. G. Nanoscale heat transfer. *Encyclopedia Nanosci. Nanotechnol.* **7,** 429–459 (2004).
2. Pop, E., Sinha, S. & Goodson, K. E. Heat generation and transport in nanometer-scale transistors. *Proc. IEEE* **94,** 1587–1601 (2006).
3. Capinski, W. S. *et al.* Thermal-conductivity measurements of GaAs/AlAs superlattices using a picosecond optical pump-and-probe technique. *Phys. Rev. B* **59,** 8105–8113 (1999).
4. Ju, Y. S. & Goodson, K. E. Phonon scattering in silicon films with thickness of order 100 nm. *Appl. Phys. Lett.* **74,** 3005–3007 (1999).
5. Chen, R. *et al.* Thermal conductance of thin silicon nanowires. *Phys. Rev. Lett.* **101,** 105501 (2008).
6. Chiritescu, C. *et al.* Ultralow thermal conductivity in disordered, layered WSe_2 crystals. *Science* **315,** 351–353 (2007).
7. Hochbaum, A. I. *et al.* Enhanced thermoelectric performance of rough silicon nanowires. *Nature* **451,** 163–167 (2008).
8. Chang, C. W., Okawa, D., Garcia, H., Majumdar, A. & Zettl, A. Breakdown of Fourier's law in nanotube thermal conductors. *Phys. Rev. Lett.* **101,** 075903 (2008).
9. Poudel, B. *et al.* High-thermoelectric performance of nanostructured bismuth antimony telluride bulk alloys. *Science* **320,** 634–638 (2008).
10. Lee, J. *et al.* Electrical, thermal, and mechanical characterization of silicon microcantilever heaters. *J. Microelectromech. Syst.* **15,** 1644–1655 (2006).
11. Hamad-Schifferli, K., Schwarts, J. J., Santos, A. T., Zhang, S. G. & Jacobson, J. M. Remote electronic control of DNA hybridization through inductive coupling to an attached metal nanocrystal antenna. *Nature* **415,** 152–155 (2002).
12. Mahan, G. D. & Claro, F. Nonlocal theory of thermal conductivity. *Phys. Rev. B* **38,** 1963–1969 (1988).
13. Chen, G. Nonlocal and nonequilibrium heat conduction in the vicinity of nanoparticles. *J. Heat Transfer* **118,** 539–545 (1996).
14. Yang, R. G., Chen, G., Laroche, M. & Taur, Y. Simulation of nanoscale multidimensional transient heat conduction problems using ballistic-diffusive equations and phonon Boltzmann equation. *J. Heat Transfer* **127,** 298–306 (2005).
15. Saha, S. K. & Shi, L. Molecular dynamics simulation of thermal transport at a nanometer scale constriction in silicon. *J. Appl. Phys.* **101,** 074304 (2007).

16. Panzer, M. A. & Goodson, K. E. Thermal resistance between low-dimensional nanostructures and semi-infinite media. *J. Appl. Phys.* **103,** 094301 (2008).
17. Chen, G. Ballistic-diffusive heat-conduction equations. *Phys. Rev. Lett.* **86,** 2297–2300 (2001).
18. Volz, S. & Chapuis, P. O. Increase of thermal resistance between a nanostructure and a surface due to phonon multireflections. *J. Appl. Phys.* **103,** 034306 (2008).
19. Prasher, R. Predicting the thermal resistance of nanosized constrictions. *Nano Lett.* **5,** 2155–2159 (2005).
20. Hasegawa, M. & Sone, Y. Rarefied gas flow through a slit. *Phys. Fluids A* **3,** 466–477 (1991).
21. Wexler, G. Size effect and non-local Boltzmann transport equation in orifice and disk geometry. *Proc. Phys. Soc. Lond.* **89,** 927–941 (1966).
22. Sverdrup, P. G., Sinha, S., Asheghi, M., Uma, S. & Goodson, K. E. Measurement of ballistic phonon conduction near hotspots in silicon. *Appl. Phys. Lett.* **78,** 3331–3333 (2001).
23. Cahill, D. G. Analysis of heat flow in layered structures for time-domain thermoreflectance. *Rev. Sci. Instrum.* **75,** 5119–5122 (2004).
24. Etessam-Yazdani, K., Asheghi, M. & Hamann, H. *Proc. HT2007-32868, ASME-JSME (Thermal Engineering Summer Heat Transfer Conference)* 349–356 (2007).
25. Rundquist, A. *et al.* Phase-matched generation of coherent soft X-rays. *Science* **280,** 1412–1415 (1998).
26. Tobey, R. *et al.* Ultrafast extreme ultraviolet holography: Dynamic monitoring of surface deformation. *Opt. Lett.* **32,** 286–288 (2007).
27. Miaja-Avila, L. *et al.* Laser-assisted photoelectric effect from surfaces. *Phys. Rev. Lett.* **101,** 113604 (2008).
28. Siemens, M. *et al.* High-frequency surface acoustic wave propagation in nanostructures characterized by coherent extreme ultraviolet beams. *Appl. Phys. Lett.* **94,** 093103 (2009).
29. Vicanek, M., Rosch, A., Piron, F. & Simon, G. Thermal deformation of a solid-surface under laser irradiation. *Appl. Phys. A* **59,** 407–412 (1994).

Acknowledgements

This work was financially supported by the DOE Division of Chemical Sciences, Geosciences, and Biosciences and the National Science Foundation Engineering Research Center for Extreme Ultraviolet Science and Technology.
R.Y. acknowledges support from NSF/CAREER (#0846561) and AFOSR/DCT (#FA9550-08-1-0078) programmes.

Author contributions

M.E.S., R.Y., Q.L., M.M.M. and H.C.K., planned the experiment. The samples were designed and fabricated by E.H.A. Experiments were carried out by M.E.S. and Q.L. All authors discussed the results, analysed the data and contributed to manuscript preparation.

Additional information

The authors declare no competing financial interests. Supplementary information accompanies this paper on www.nature.com/naturematerials. Reprints and permissions information is available online at http://npg.nature.com/reprintsandpermissions. Correspondence and requests for materials should be addressed to M.E.S.